Acoustic Emission Wave Propagation in Honeycomb Sandwich Panel Structures

Ahmed H. Abdulaziz[a], Mohammed Hedaya[a], Adel Elsabbagh[a], Karen Holford[b], John McCrory[b*]

[a] Design and Production Engineering Department, Faculty of Engineering, Ain Shams University, Abbaseya, 11517, Cairo, Egypt

[b] Cardiff University School of Engineering, The Parade, CF24 3AA, Wales, UK

Abstract

This paper studies acoustic emission (AE) wave propagation in a glass fibre aluminium honeycomb sandwich panel (HSP). Of particular novelty is the quantification of the through-thickness propagation of AE from one surface of the HSP to the other, which is a real-world monitoring consideration for applications where AE instrumentation is only be permissible on one surface, i.e. aerofoils. Complexity was introduced to the specimens in stages to enable a thorough understanding; first investigating propagation in a large glass fibre laminated plate (GFLP) alone; then in bespoke sandwich specimens with a limited number of honeycomb cells; and, finally, in a large HSP. The results of this paper demonstrate that, whilst some energy is transmitted through the honeycomb core, AE propagating in an HSP becomes bound in the outer plates. Despite this, propagation in these outer plates differs to that in an equivalent plate of the same material in isolation due to the complex interactions with the structural elements of the HSP. Further, propagation of AE transmitted from one surface to the other was quantified for the first time, giving insight into expected attenuation rates and characteristics for practical applications.

Keywords: Acoustic Emission; Propagation; Glass Fibre Composites; Insertion Loss; Lamb Wave; Honeycomb Sandwich Panel

Corresponding Author: John McCrory, Cardiff University School of Engineering, CF24 3AA
– Email Address: mccroryjp@cardiff.ac.uk
– Phone: +44 (0)29 2087 5924

1. Introduction

A honeycomb sandwich panel (HSP) is a composite structure combining two stiff thin plates bonded to a honeycomb core, often made from either aluminium, aramid or nomex [1–2]. As the demand for light-weight materials whose stiffness can be tailored increases, the use of honeycomb composite structures becomes of a greater interest [3–4] due to their advantageous mechanical properties, including high bending and compression stiffness with light weight, and manufacturing flexibility [5]. However, due to their complex nature, HSPs can experience a wide range of damage mechanisms such as yielding or wrinkling of plates, intra-cell dimpling, matrix cracking, local indentation, plate-honeycomb de-bonding and core shearing [6]. This poses challenges for conventional non-destructive testing and structural health monitoring (SHM).

Acoustic Emission (AE) monitoring is suited to SHM applications such as wind turbines, where structures can be remote or difficult to monitor. AE refers to transient or continuous elastic waves resulting from a rapid release of energy from a highly strained zone within a material under loading or in service [7], and AE monitoring refers to the detection of these waves to infer information about the structure [8]. The use of an array of sensors allows AE sources to be located, and the AE waveforms themselves can give an insight as to the defect mechanism, further increasing the desirability to implement AE monitoring [9]. However, AE is a complex phenomenon, particularly in composite materials, and reliable AE monitoring relies on a thorough understanding of the nature of AE wave propagation, its attenuation, its directional velocities and the frequencies [10,11].

In thin plates and shell structures, the elastic AE waves are bound by the surfaces and propagate as Lamb waves. Lamb waves consists of two main characteristic modes; symmetric (i.e. extensional, S_o) and anti-symmetric (i.e. flexural, A_o) [12]. However, structural complexities, such as those found in an HSP, have the potential to change or distort the nature of the elastic waves, and, to date, AE propagation in HPSs has seen far less academic attention than other composite structures. Thus, propagation in HSPs is not currently understood to a sufficient level for confident AE-based SHM implementation. This study adds to the collective knowledge in this field, and makes several astute observations about the complex interactions occurring during AE propagation in glass fibre aluminium-honeycomb sandwich panel structures.

AE in glass fibre composites panels is understood reasonably well, with recent publications focusing on characterising damage mechanisms [13][14]. With regards to propagation, Hafizi and Epparachchi [15] studied AE attenuation using Hsu-Nielsen (H-N) sources in a 400 x 400 x 2.9 mm glass fibre reinforced epoxy plate made by hand layup of $[0^o]_4$ laminates in directions 0^o, 45^o, 60^o and 90^o and found that Lamb waves propagated with approximate frequencies of 30 kHz and 100 kHz for A_o and S_o, respectively.

Wu et al. [16] studied AE wave velocity in honeycomb sandwich structures, consisting of CFRP and woven glass fibre laminates skins with a balsa core, numerically using

the plate wave theory and experimentally using Hsu-Nielsen (H-N) sources. However, their focus was on the time of arrival of the acoustical wave which was used to determine the velocity of the extensional mode without decomposing the signal into its two indicative modes (i.e. flexural and extensional modes). Through this, they found that the extensional mode velocity was dependent on the direction of propagation with respect to the fibre alignment in the plate. Sikdar et al. [17] studied AE wave propagation analytically and experimentally in a sandwich structure which consisted of an aramid honeycomb core with two aluminium skins in order to implement a particle swarm optimised source location.

Guo et al. [18] studied Lamb wave characteristics in aluminium honeycomb structure using a multilayer model and found that the phase and group velocity in dispersion curves of the Lamb waves are less affected by the core properties at low frequencies, while attenuation is increased at higher frequencies. Baid et al. [19] studied the dispersion characteristics of Lamb waves in a sandwich structure consisting of 12.7 mm aluminium honeycomb with two woven carbon fibre plates. They used a global matrix method to determine the dispersion curves and validated their solutions experimentally using a pair of piezoelectric transducers (PZT) on the top plate. Only the flexural A_o mode velocities were obtained experimentally with a good agreement with the analytic solution.

Despite its importance as a real-world monitoring consideration, across all literature studied none quantified the propagation behaviour of AE through the thickness of the sandwich panel, from one surface to the other. Propagation of this nature would be present if AE transducers were affixed to the inside skin of an aerofoil HSP structure, such as a wind turbine blade, yet damage could occur on the outer skin. Figure 1 gives an example of this, showing an aerostructure where the AE sensors are mounted from inside, as it is impractical to mount the sensors on the outer skin. This through-thickness propagation is a mechanism which this paper looks to quantify, by investigating AE propagation in a glass fibre aluminium honeycomb sandwich panel structure.

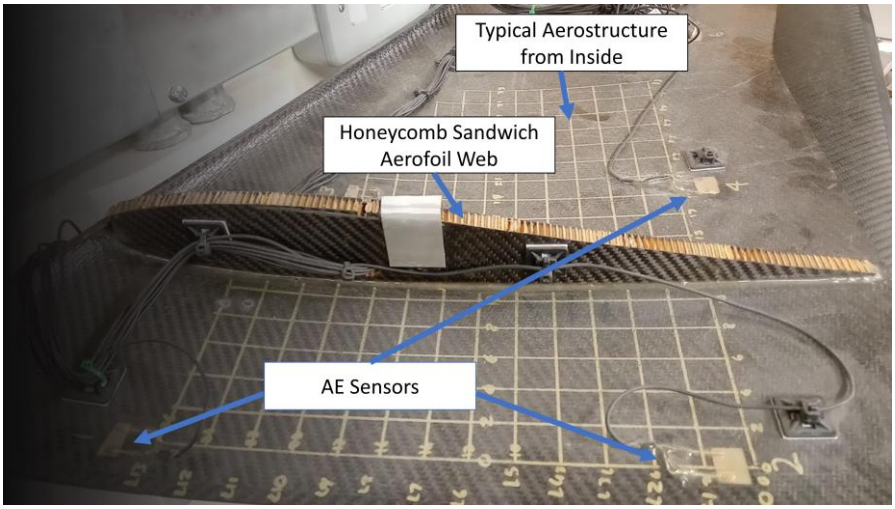

Figure 1. Example of AE sensors inside an aerostructure

In order to fully appreciate the changes introduced by the addition of the honeycomb core, this study builds complexity in the specimen in stages; starting with an investigation of AE wave propagation in a glass fibre laminated plate (GFLP); then in bespoke HSPs with a limited number of honeycomb cells; and finally in a full sized HSP. The progression of objectives of the article are as follows:

- Investigating AE propagation in a 820 x 820 mm glass fibre plate.
- Investigating AE propagation from one surface of a sandwich panel to the other using bespoke honeycomb sandwich panels (200 x 75 mm) with a limited number of cells; starting with a single honeycomb cell and working up; hence, the nature of transmitted AE can be quantified.
- Investigating AE propagation in a full-scale (820 x 820 mm) honeycomb sandwich panel, including the through-thickness response, and relating these findings back to propagation in pure glass fibre and the learnings from the bespoke specimens.
- Proposing the ‘’insertion loss’’ concept to describe the difference between the AE wave propagation in the glass fibre plate before and after bonding the honeycomb layer.

This paper is divided into four further sections. Section 2 describes the specimen preparation. Section 3 presents wave propagation studies in a single GFLP, bespoke HSP specimens, and the large HSP. Section 4 presents and discusses the results and finally the conclusions are drawn in section 5.

2. Specimen Preparation

2.1. Glass Fibre Laminated Plate

Three 820x820 mm GFLPs were manufactured, using unidirectional glass fibre fabric from Cristex Composite Materials, Ltd., by vacuum assisted resin infusion. The glass fibre

fabric was laid up in a [0°/90°/0°/90°/0°] configuration. The epoxy resin (type: IN2 Epoxy, Easy Composite Ltd.) was vacuum pumped to -1000 mbar. A 5-minutes leakage test was conducted to inspect the sealing quality; the pressure drop was less than 4 mbar. Each GFLP was cured at room temperature for 24 hours resulting in an approximately 2.5 (±0.3) mm thick plate. Figure 2 presents the manufacturing process. Post manufacturing, an ultrasonic phased array inspection, using an Olympus-MX2, was conducted to ensure that there were no significant manufacturing defects.

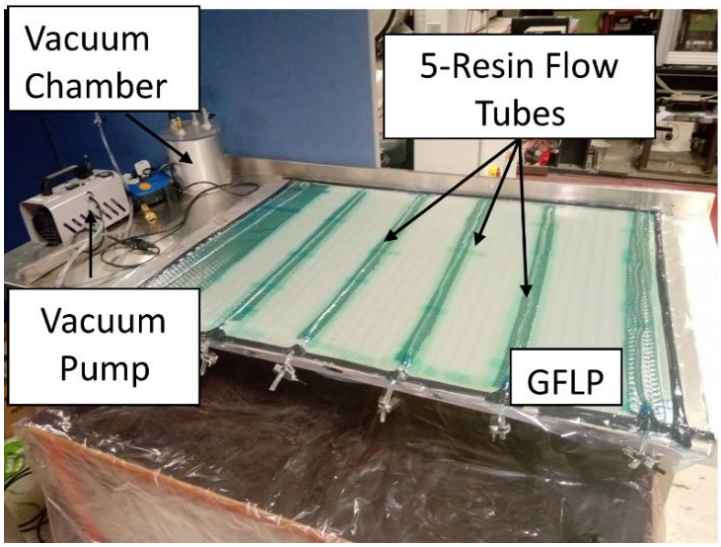

Figure 2. The resin infusion manufacturing process of GFLP

2.2. Bespoke Deducted Honeycomb Sandwich Panels

In order to study the transmission of AE through the honeycomb cells, from one surface of an HSP to the other, bespoke specimens were manufactured with a deducted number of honeycomb cells. Each bespoke specimen consisted of two GFLPs of 200 x 75 mm, with a limited number of aluminium honeycomb cells between them; 1, 2, 3, 4, 5, 6, 7, and 10. The aluminium honeycomb was purchased from Easy Composite Ltd, with a height of 10 mm, cell size of 6.4 mm, wall thickness of 0.075 mm, and manufactured from 3003 series aluminium alloy. The GFLP construction was the same as that in the previous section, with a thickness is 2.5mm. Permabond ET-538 was used to bond the honeycomb cells to the plates. Specimens with different numbers of cells were created to understand the effect of cell number on the transmitted AE, allowing for a more thorough understanding of propagation in the full-scale HSP. Figure 3 shows the schematic drawing of the bespoke specimen, and Tables 1 and 2 present the mechanical properties of the honeycomb sandwich panel and aluminium honeycomb core.

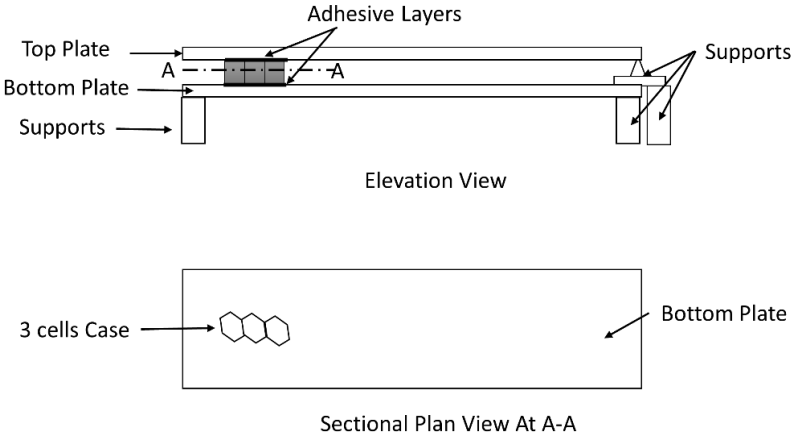

Figure 3. Schematic of bespoke HSP specimen with three cells

Table 1. Mechanical properties of the sandwich panel

Layer	E_1 (GPa)	E_2 (GPa)	E_3 (GPa)	G_{12} (GPa)	υ_{12}	υ_{13}	P (kg/m^3)	V_{fibre} %	V_{matrix} %	Thickness (mm)
GFLP-Skin	37.5	13	13	4.8	0.265	0.26	1875	55	45	0.5
Adhesive	3	3	3	-	0.28	0.28	1100	-	-	0.25

Table 2. Mechanical properties of the aluminium honeycomb core

Compressive Strength (Stabilised)	4.52	MPa
Plate Shear Strength (lengthways)	2.48	MPa
Plate Shear Modulus (lengthways)	448	MPa
Plate Shear Strength (widthways)	1.45	MPa
Plate Shear Modulus (widthways)	241	MPa
Density	83	Kg/m^3

2.3. Honeycomb Sandwich Panel

A large honeycomb sandwich panel HSP was manufactured to study the AE propagation in such a structure. The overall size of the HSP is 820 × 820 × 15 mm with thickness of each GFLP 2.5mm and height of the aluminium honeycomb equal to 10mm.

The aluminium honeycomb was the same as that in the bespoke specimens, and the GFLP manufacture has already been described. The honeycomb was bonded between the GFLPs using the Permabond ET-538, and cured under compression for 24 hours. Figure 4 presents the geometric features of the panel.

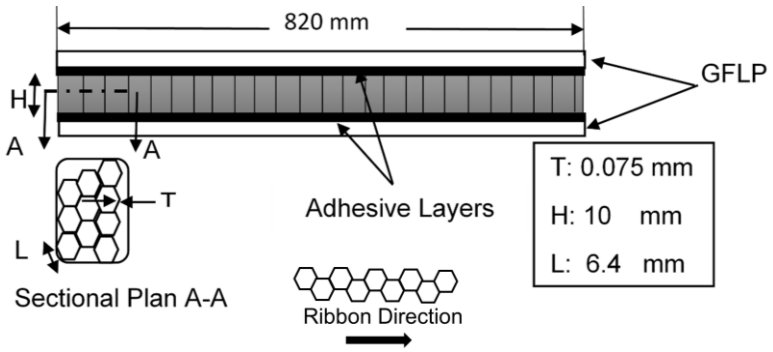

Figure 4. Schematic of HSP structure

3. Experimental Procedure

3.1. Wave Propagation using Hsu-Nielsen sources

3.1.1. GFLP

The frequencies, attenuation properties, and velocities of AE in the GFLP were all investigated. Since AE is affected by fibre orientation, the study was conducted across a range of directions, from 0° to 90° with 15° intervals [±1°]. H-N sources were generated five times at each testing point, with testing points spaced at 50 mm intervals from the sensor along each of the tested directions, as shown in Figure 5. Two wideband, MISTRAS Group, Ltd (MGL), WD sensors (100 – 1000 kHz) were bonded to the GFLP. The first sensor, S_1, was bonded using silicon at the GFLP's centre and the second, S_2, was bonded by grease at a distance 100 mm behind S_1. AE timing parameters (selected by trial and error) were 100, 250, and 500 µs for the PDT, HDT and HLT, respectively. Preamplifier gain was 40 dB, frequency range 20kHz to 1200 kHz, threshold level 40 dB and the sampling rate 5 MHz.

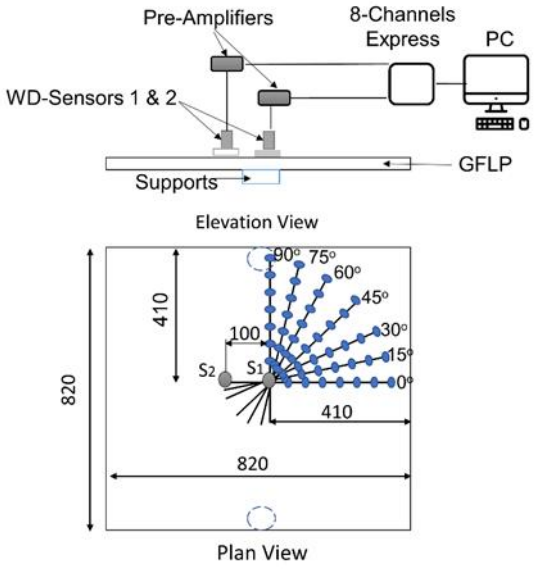

Figure 5. GFLP propagation experimental setup (dimensions in mm)

3.1.2. Bespoke HSPs

To investigate the transmission of AE from one plate to another through the honeycomb cells, a study was carried out using bespoke HSP specimens of 200 × 75 × 2.5 mm, each with a different number of cells. For each bespoke HSP, five H-N events were generated on the bottom plate, a short distance from the honeycomb cell(s), whilst AE was recorded by a WD sensor bonded to the top plate, using silicone, as shown in Figure 6. AE timing parameters were 100, 200, and 400µs for the PDT, HDT and HLT, respectively. The preamplifier gain was 40 dB, frequency range 20kHz to 1200 kHz, threshold 40 dB and sampling rate 5 MHz.

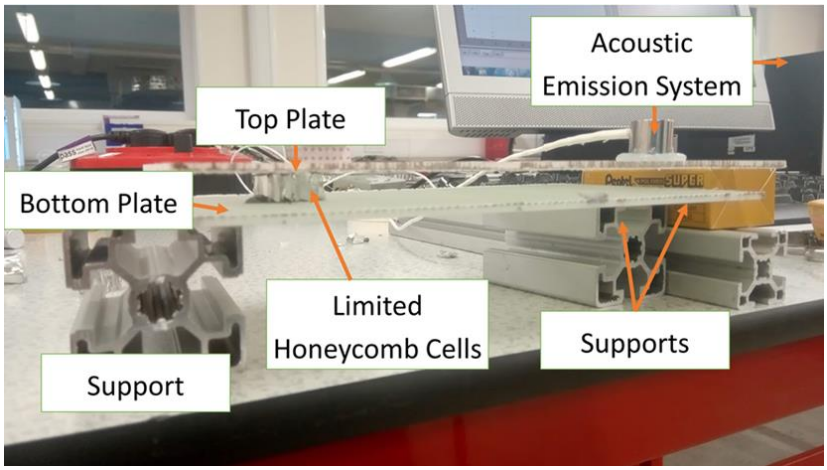

Figure 6. AE wave propagation test setup for bespoke HSPs

3.1.3. HSP

The propagation study on the large HSP was conducted following a similar procedure to that used on the GFLP; two WD sensors were bonded to the top GFLP, where the H-N sources were generated, and an additional WD sensor was bonded onto the bottom GFLP of the HSP to record energy transmitted through the honeycomb layer, as shown in Figure 7. AE recording parameters were 100, 200, and 300µs for the PDT, HDT and HLT, respectively. The preamplifier gain was 40 dB with a frequency range from 20kHz to 1200 kHz. The threshold level was 40 dB and sample rate 5 MHz.

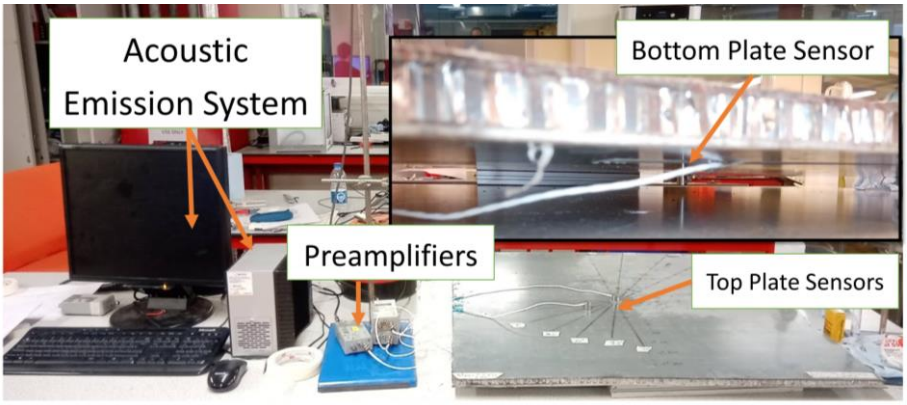

Figure 7. Experimental setup for AE propagation study on the HSP

3.2. Laser Vibrometry Scanning (LVS) Method

LVS was carried out on both the GFLP and the HSP covering the angles from 0° to 90° with 15° increment in both cases as for the H-N study. The aim of this experiment is to confirm the nature of the AE wave propagation in the GFLP and the HSP from the surface movement directly, without the frequency biases of the recording sensor.

3.2.1. GFLP

A Broadband PZT (AGU Vallen-VS-900-M) with a non-integrated pre-amplifier and 100 – 900 kHz response range was placed in the centre of the GFLP. A 5-cycle sinusoidal burst from a function generator (WaveStation 2012) with a frequency of 300 kHz and peak-to-peak voltage 3 V_{pp}, amplified by ×100 by amplifier (Model 7500 amplifier-Krohn-Hite, Ltd), was input as an excitation signal to the PZT. A 3D-LVS (Polytec-PSV-500) was used for scanning the velocity field, as shown in Figure 8. Sampling frequency was 2560 kHz, satisfying the Nyquist–Shannon sampling theorem to obtain a good reconstruction of the signals. The number of scanning points was 174 in each direction, with 1200 measurements taken at each point and averaged to improve the signal-to-noise ratio.

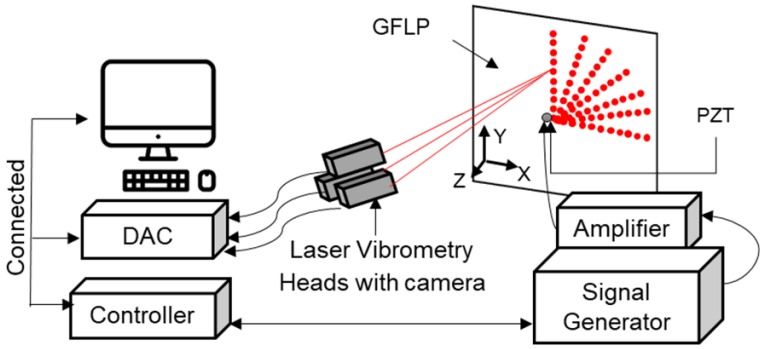

Figure 8. Schematic drawing of Laser vibrometry scanning of GFLP

3.2.2. HSP

The Scanning Laser Vibrometry setup used for the HSP was similar to that used for the GFLP, but as the honeycomb core increased the in-plane and out-of-plane stiffness, the PZT (AGU Vallen-VS-900-M) was replaced with (MGL -R6α- transducer) with a lower frequency range (35-100) kHz. This was attached to the front surface of the panel to study wave propagation at 80 kHz of excitation in order to obtain a better separation between Ao mode and So mode, and the back sensor was excited at 40 kHz to analyse the waveforms on the front plate resulting from the energy transmitted from back plate to front plate through the honeycomb cells; these frequencies were selected through trial and error. The number of scanning points in each direction was 175, with 1500 measurements taken at each point and averaged to improve the signal-to-noise ratio.

4. Results and Discussion

4.1. Propagation Study

4.1.1 Bespoke HSPs

In order to clearly understand wave propagation in the full-scale honeycomb sandwich panels, wave propagation through a limited number of cells was first studied. It was discovered that enough energy was transmitted through the honeycomb cell(s) for an event generated on the bottom plate to be detected by the AE sensor on the opposing, top plate. Figure 9 shows examples of AE hits recorded from the top GFLP arising from H-N sources generated on the bottom GFLP for several samples, each with a different number of cells. Due to the plate geometry, stiffness, and the guided wave effect, the energy arriving in the top plate formed Lamb waves. It can be seen that the amplitude of the S_o mode is vastly lower than that of the A_o mode, barely visible above the noise, though distinguishable in the frequency spectrum.

To assist interpretation, Figure 9 includes a magnified image of the S_o mode arrival, as well as frequency spectra for each of the waveforms displayed. The disparity in the amplitudes of the two modes observed is likely due to the out-of-plane nature of the energy transfer from the honeycomb cells to the upper plate, resulting in larger amplitude out-of-plane, A_o mode. For smaller numbers of cells, the propagation frequencies of the A_o and S_o modes of this transmitted energy are centred around 30kHz and 90kHz respectively, which we will later learn is also their propagation frequencies in the GFLP alone. However, as the number of cells is increased, Figure 9d, the A_o mode frequency range descends slightly, with two, more pronounced peaks forming between 15 and 30 kHz.

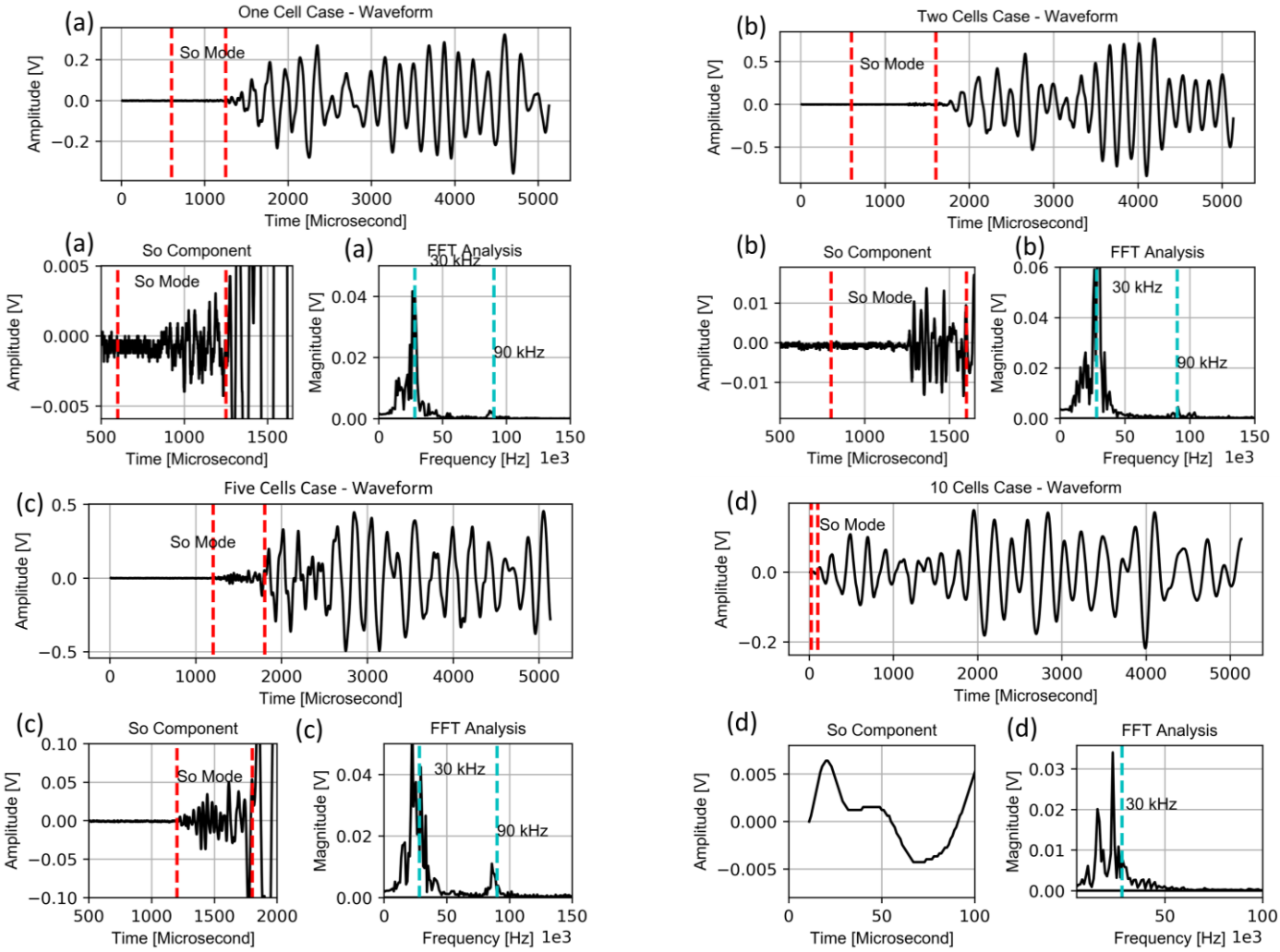

Figure 9. Waveforms, FFT, and zoomed-in S_o region in (a) one cell case, (b) two cells case, (c) five cells case and (d) ten cells case

When considering a small number of cells, the amplitude of the Lamb waves in the top plate increases in line with the number of cells as a result of the increase in energy transfer from the bottom plate; the relationship between the number of cells and the energy of the AE hit recorded is given in Figure 10. Curiously, as the number of cells is increased further, the energy of the AE hit received by the sensor on the top plate diminishes; it is hypothesised that this is because, once the honeycomb cells span a large enough surface area of the panel, it is possible for energy transmitted to the top surface to leak back into the honeycomb cells which lie ahead of its propagation path. Of additional interest is the observation that the S_o energy increases to its highest level at six cells, and then begins to drop, whereas the A_o energy reaches its highest level at five cells before dropping. This difference could be owed, once again, to the out-of-plane nature of the A_o mode, making it more susceptible to re-transmitting into the honeycomb cells.

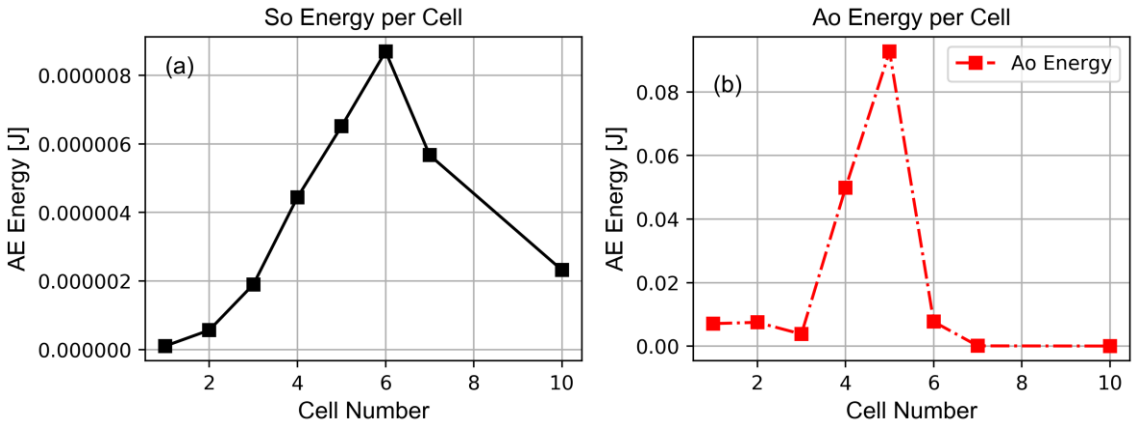

Figure 10. Transmitted (a) S_o and (b) A_o energy for bespoke HSPs with different numbers of cells

4.1.2. Frequency and Velocity Measurements

As expected, AE propagated in the GFLP as Lamb waves. An examples of an AE waveform and its frequency spectra from an event generated in the 0° direction, at a distance of 50 mm from the AE sensor, can be seen in Figure 11a for the GFRP. The A_o and S_o modes have dominant frequencies centred at 30 kHz and 90 kHz respectively which conforms to the findings of Hafizi et al [15]. Data recorded from the HSP was investigated in a similar way but using signals from both the top plate, where the H-N source was generated, and the bottom plate, where AE energy had transmitted through the aluminium honeycomb core. Figure 11b shows waveforms recorded from the sensor on the top plate of the HSP in the 0° direction at 50 mm from the sensor demonstrating clear evidence of Lamb wave propagation. The frequencies of the A_o and S_o modes were centred at 30 kHz and 90 kHz, as in the case of the GFLP alone; though the signal was attenuated as a result of energy loss into the honeycomb core. For the bottom plate, Figure 11c shows example of waveform recorded from the sensor on the bottom plate of the HSP in the 0° direction at 50 mm from the sensor. It can be seen that the amplitudes are dramatically lower those recorded on the top plate, due to the limited amount of transmitted energy. As expected from the observations made on the data collected from the bespoke HSP samples, the energy transmitted to the bottom plate of the HSP forms Lamb waves with a heavy bias towards the A_o mode, and with two distinctive frequency peaks between 15 and 30 kHz. Only a very small high frequency S_o component, centred at 90 kHz, can be seen in the frequency spectrum. The frequency characteristics of AE in the other direction tested were similar to those exemplified here.

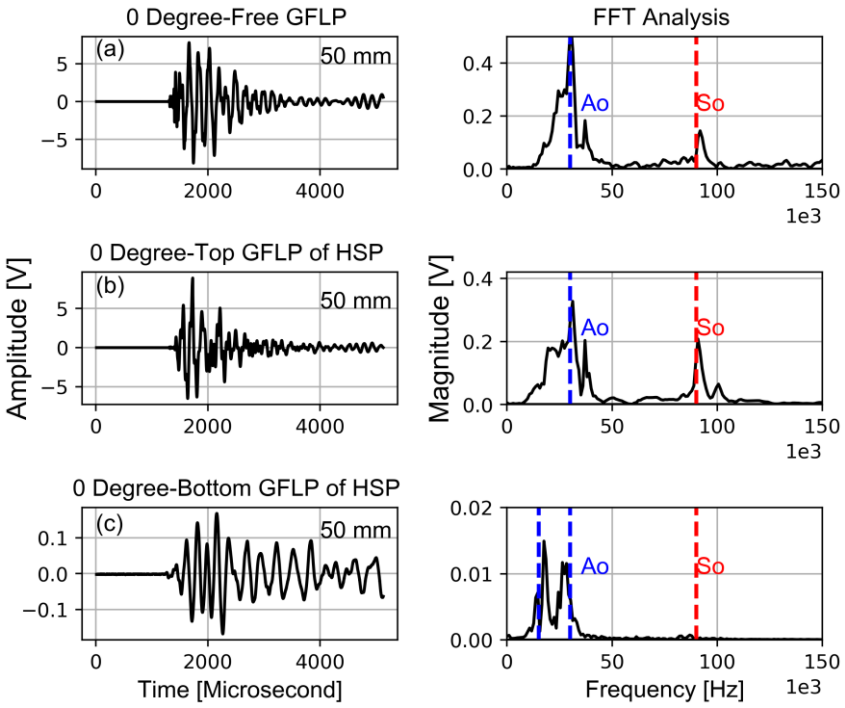

Figure 11. Waveforms in time and frequency domains for 0° direction at 50 mm, recorded on (a) GFLP alone, (b) top plate of the HSP, and (c) bottom plate of the HSP

In order to calculate the velocities of the two modes, it is necessary to know their arrival time at each sensor. To avoid manual interpretation, handpicking, or utilising a threshold crossing method, all of which can be prone to errors [20], the Akaike Information Criterion (AIC) [21] method was used to determine an accurate first arrival time of both Lamb wave modes [19][20]. The AIC [21] compares the similarity between signal parts before and after point (n) until it reaches the minimum similarity value (and hence the signal onset is effectively determined. Eq. (1) shows the AIC function.

$$AIC(n) = n \log(var(y(1:n))) + (n_{sample} - n - 1) \log(var(y(n+1: n_{sample}))) \quad \text{Eq.(1)}$$

where y(1, n) (for data points starting from 1 to n) and y (n+1: n_{sample}) (for data points n + 1 to n_{sample}) are the two segments in the selected time window, and (var) stands for the statistical variance of the data. Figure 12 shows an example of the application of AIC function (red line) and Figure 13 shows the whole signal processing sequence. It should be noted that in order to utilise the AIC function to identify the onset of the A_o mode, the signal was first passed through a fourth order low pass Butterworth filter with a normalized cut off frequency at 45kHz, to eliminate the S_o mode energy. White Gaussian Noise (WGN) was then added to this filtered signal to mimic the unfiltered AE signal [22] and allow the AIC function to calculate the arrival time of A_o mode.

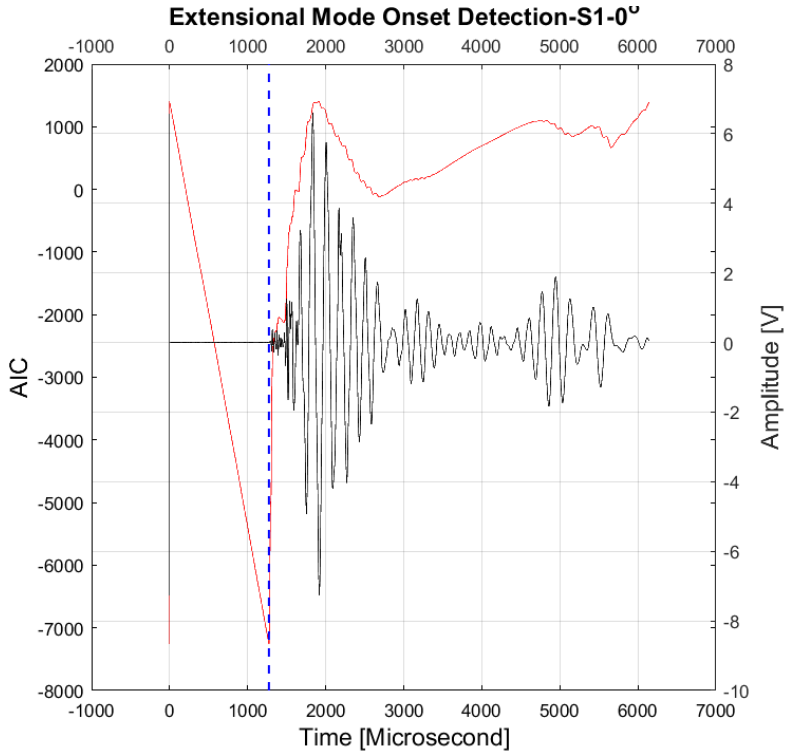

Figure 12. Example of the time of arrival determination for S_o mode in 0° using AIC

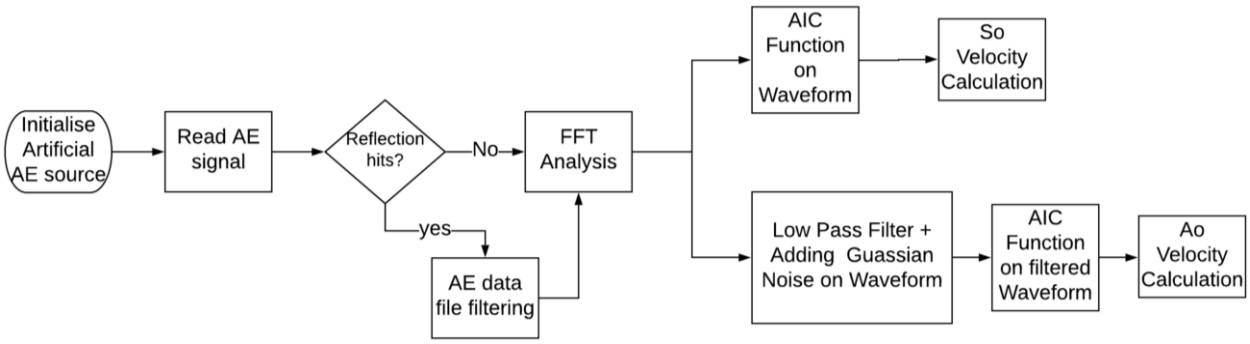

Figure 133. Velocity calculation code flow-diagram

With accurate arrival times known, the velocities of each mode were calculated for each direction tested, for both the GFLP and the HSP, by dividing the difference in the time of arrival of the signal at sensors 1 and 2 by the distance between them, see Figs 4 and 6 for reference; the results of this process can be seen in Figure 14. In-line with to the work of Wu et al.[16], in the GFLP, the maximum group velocities of the S_o mode were found to be 4028 (± 9.64) m/s and 4005 (± 15.76) m/s in 0° and 90° directions respectively; and the minimum group velocity was found to be 3472 (± 10.35) m/s in the 45° direction. This trend is expected as the S_o mode propagates with radial in-plane motion [26], thus, its velocity is proportional to the in-plane stiffness, increasing as the wave propagates in the fibre direction and decreases when it propagates perpendicular to the fibre direction [27]. Conversely, the velocity of the A_o mode is independent of the fibre orientation as it

propagates with out-of-plane motion, thus its velocity is linked to the out-of-plane stiffness [23]. Thus, the A_o velocity exhibits a flat velocity profile in the GFLP, with an average value of 1323 (± 58) m/s.

The velocity results for the HSP, in Figure 14b, show that the addition of the sandwich structure had a notable effect on the velocity of the S_o mode. The maximum S_o velocities in the HSP are 3927.22 (±8.28)m/s and 3892.76 (±15.42)m/s in the 15° and 75° directions, respectively, with the velocity gradually diminishing either side of these directions. Of note to understanding the potential reason for this is that the honeycomb core has increased stiffness along its ribbon direction, and the angle between one ribbon direction and the next in hexagonal honeycomb is 60°. Thus, it could be hypothesised that the S_o velocity has a dependency on the ribbon direction of the honeycomb core, as the 60° separation in the directions of the maximum S_o velocities matches the 60° angle between the ribbon directions, suggesting that the cells could act as a waveguide for the S_o mode; however, this interaction would requires more experimentation to understand. On the other hand, the S_o velocities in 0° and 90° drop to 3637.36 (±33.97) m/s and 3752.15 (±9.02) m/s, respectively, which can be attributed to the energy scattering into the honeycomb cells [28]. The A_o velocity remains largely unchanged in the top plate of the HSP when compared to the GFLP alone, with an average of 1290 (±86.5) m/s. This is striking as the purpose of the honeycomb layer is to increase the out-of-plane stiffness of the whole panel, though insight could be gained here by considering the scale at which the stiffness change occurs, i.e. macro vs micro.

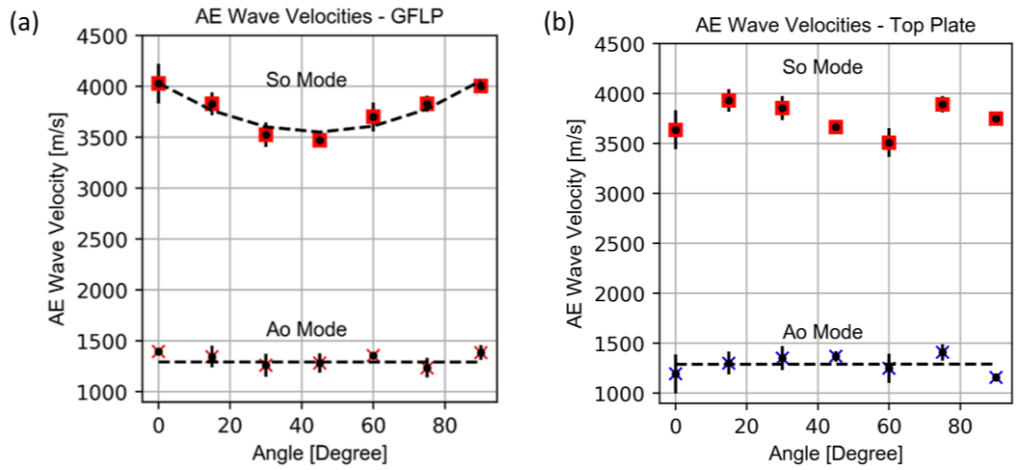

Figure 14. Lamb wave group velocities on (a) GFLP and (b) Top plate of HSP

The dispersive behaviour of the two Lamb wave modes was also investigated in both the GFLP and HSP. First, the dispersion curves for each propagation direction in glass fibre were calculated theoretically using LAMSS-COMPOSITE software [29]; an example of the results of this for the 0° direction can be seen in Figure 15, given by the dashed lines. It is worth noting that the glass fibre model in LAMSS-COMPOSITE was woven, however, its stiffness matrix was comparable to that of the unidirectional GFLP used in this study. It has

already been established that the propagating frequency of the S_o mode centred at 90 kHz; given the GFLP thickness of 2.5 mm, this results in a frequency-thickness of 225 kHz.mm. Referring to the theoretical S_o dispersion curve in Figure 15, at frequency-thickness 225 kHz.mm, the S_o mode velocity is 3775 m/s; this is in-line with the group velocity of the S_o mode found experimentally in the corresponding direction, with an error of 3.8%. Following a similar process for the A_o mode, it has been established that the propagating frequency is centred at approximately 30 kHz, resulting in a frequency-thickness of 75 kHz.mm. The theoretical dispersion curve in Figure 15 shows the A_o velocity to be 1185m/s for this frequency-thickness. This is comparable to the A_o group velocity determined experimentally, with an error of 8%. Figure 15 also displays the experimentally determined dispersive properties of the two Lamb wave modes in the GFLP, in the 0° direction. These were obtained for each direction through application of narrow band-pass frequency filters (5 kHz width) to the recorded waveforms at 10 kHz intervals between 20 and 120 kHz, and subsequent determination of the arrival time of each filtered mode using AIC. This allowed the time of flight of each filtered mode to be determined between the two recording sensors and, thus, calculation of the velocity of both modes specific to each frequency (frequency-thickness). To allow for sufficient separation of the two primary Lamb wave modes in this process, only the data from the events generated at 300 mm from the sensors were used. It can be observed that the experimentally determined dispersive properties of the S_o mode in the GFLP are in line with theoretical expectations. The dispersive properties of the A_o mode have good agreement with the theoretical curve at lower frequency-thickness values, however calculation of the A_o velocity became less reliable at higher frequencies due to the limited flexural energy at those frequencies and attenuation obfuscating arrival time detection.

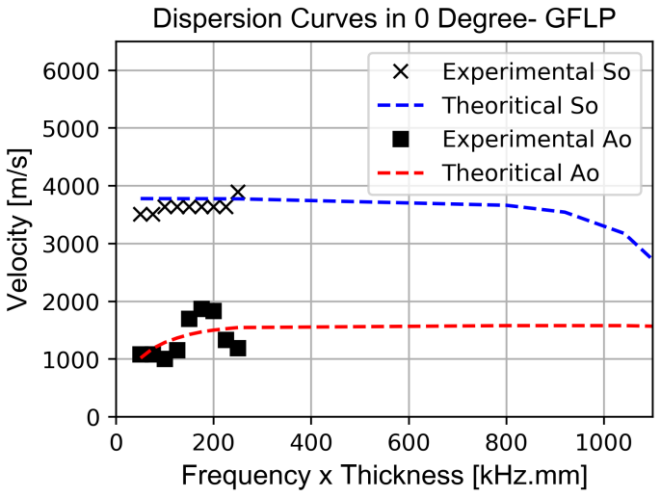

Figure 15. Theoretical dispersion curves for 0° direction on the free GFLP

The S_o and A_o mode dispersion curves were also calculated from the experimental data collected from the top plate of the HSP, for each direction tested. Figure 16 shows an example of the results of this process for the 0° direction, alongside the theoretical

dispersion curve for glass fibre. As with the AE collected from GFRP, the higher frequency A_o components were increasingly difficult to compute; this was further exacerbated by the attenuation introduced by the honeycomb structure, hence why there are fewer data points for the A_o mode in Figure 16. As expected, there is a greater departure of the experimentally determined dispersive behaviour of both modes in the top plate of the HSP from the theoretical curve for glass fibre.

The velocity results shown in this section highlight that, whilst AE in the top and bottom plates of the HSP becomes bound and propagates as Lamb waves, the propagation characteristics of those Lamb waves have distinct differences to those in a monolithic GFLP of the same dimensions.

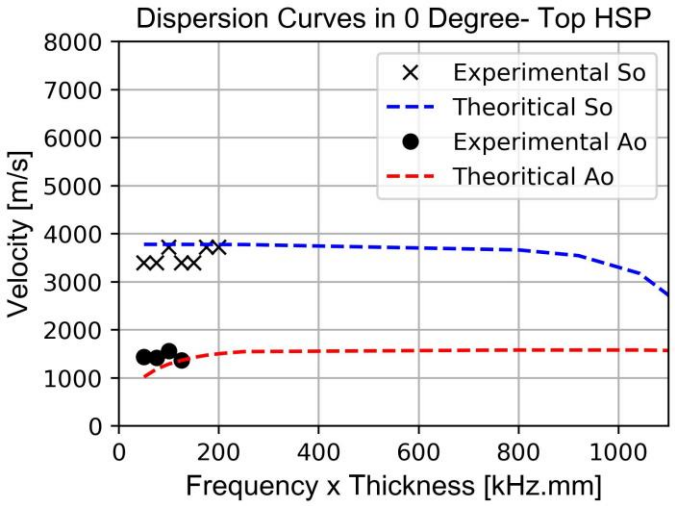

Figure 16. Theoretical dispersion curves for 0° direction on the free GFLP

4.1.3. Attenuation Measurements

AE attenuation is dramatically increased after bonding the honeycomb layer, as energy scatters or leaks into the cells, conforming with expectations and the findings of Song et al. [28]. Figure 17 shows the energy of AE hits recorded at different distances in the GFLP, and the top and bottom plates of the HSP. As expected, there is a large loss in energy of the received signal when the propagation path includes transmission through the honeycomb cells to the opposing side of the HSP.

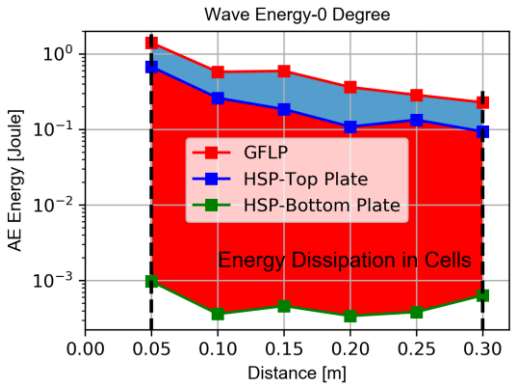

Figure 177. Energy dissipation between GFLP, top and bottom plates of the HSP

Looking more specifically the signal amplitudes, Figure 18 compares waveforms recorded from the GFLP (peak 6.584V), and top plate (peak 3.781V) and bottom plate of the HSP (peak 0.0796V); all from events generated along the 0 degrees direction at 100mm from the sensors. As expected, the amplitude of the hit from the GFLP alone is the greatest, followed by that from the top plate of the HSP (the plate the source was generated on), followed by that from the bottom plate of the HSP.

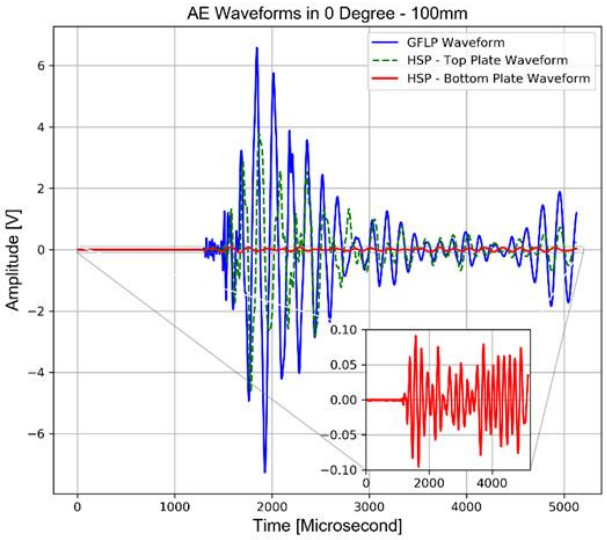

Figure 18. AE waveforms from events generated along 0° direction at 100 mm from receiving sensors

Since there is a change in the AE signal amplitude after the addition of the honeycomb layer, the concept of 'insertion loss' could be introduced to describe the effect. In telecommunication, the insertion loss is defined as the signal power loss after inserting a component or network in the transmission line[30]. Eq. (2) presents the insertion loss equation.

$$\text{Insertion loss} = 10 \times \log \frac{P_{\text{before adding device}}}{P_{\text{after adding device}}} = 20 \times \log \frac{V_{\text{before adding device}}}{V_{\text{after adding device}}} \quad \text{Eq.(2)}$$

where $P_{before\_adding\_device}$ is the signal power before inserting the component or network, $P_{after\_adding\_device}$ is the signal power after inserting the component or network, $v_{before\_adding\_device}$ is the signal voltage before inserting the component or network, and $v_{after\_adding\_device}$ is the signal voltage after inserting the component or network.

By analogy, AE propagating in a composite plate will be affected after inserting the honeycomb and bonding it to the second composite plate to form the HSP; the insertion loss could be used to describe the severity of the change. Following this line of thinking and maintaining the form of Eq. (2), $V_{\text{before adding device}}$ would be considered as the peak voltage of the AE hit recorded from the GFLP alone, and the $V_{\text{after adding device}}$ becomes the peak voltage of a hit recorded from the top panel of the HSP.

By applying this process to the waveforms, comparing AE from the GFLP alone and the top GFLP of the HSP, the insertion loss is 4.8 dB. The same approach can be used to compare AE from the top GFLP of the HSP, where the source was generated, and the bottom GFLP of the HSP, which received transmitted energy, resulting in an insertion loss of 33.5 dB. Therefore, the peak amplitude of a wave propagating 100 mm will drop 4.8 dB due to bonding the honeycomb and second GFLP to the top GFLP; and the peak amplitude of a wave propagating 100 mm and transmitting from one side of the HSP to the other will drop by 33.5 dB.

Figure 19 presents the attenuation behaviour of the S_o and A_o modes for the 0^o and 45^o directions in the GFLP and HSP. Since the S_o mode of the hits recorded on the bottom, receiving, surface of the HSP was undiscernible above the noise, its amplitude could not be reliably identified, thus, only the A_o of the bottom surface is considered. The gradient of the best fit lines for each direction were also calculated, to give the overall attenuation of the signal with distance without removing geometric spreading effects; the results of this can also be seen in Figure 19. Note that, as the amplitudes are presented in dB, the trend line equation which used in the calculations is presented by Eq.(3)

$$A = -\alpha x + c \qquad \text{Eq.(3)}$$

where;

A: Amolitude of A_o or S_o.

α: Attenuation coefficient dB/m.

x: The distance of the AE source from the receiving sensor.

c: The interception of the trending equation with the Y- axis.

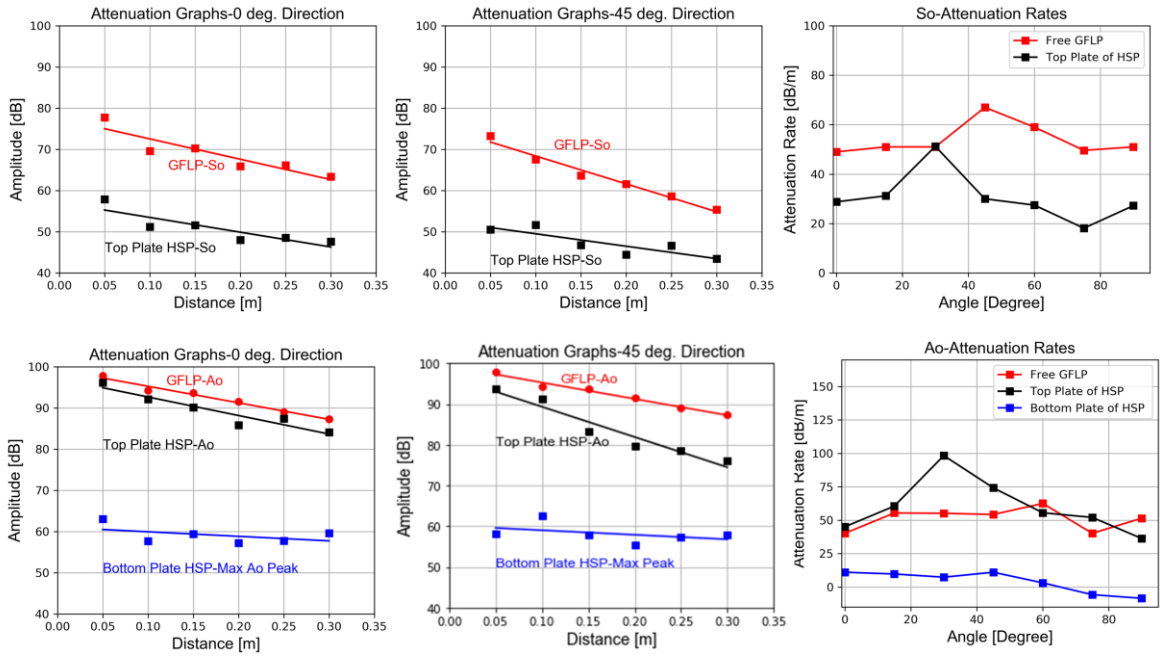

Figure 19. Attenuation behaviour of S_o and A_o for GFLP (red), HSP's top plate (black) and HSP's bottom plate (blue) for 0° and 45°, and their attenuation rates for different directions

The attenuation behaviour of both Lamb wave modes in the GFLP alone is as expected; despite the greater dispersion of the A_o mode [31], the S_o mode experiences greater attenuation due to its higher frequency [32]; the S_o mode also experiences greater directional dependency due to the increase in scattering which occurs when propagating off-fibre direction [33]. A drop in the amplitude of both wave modes can be seen as the structural complexity increases from a thin GFLP to a complex HSP, as described by the aforementioned insertion loss. When comparing amplitudes in GFLP to those in the top plate of the HSP, the higher frequency, S_o mode diminished by a greater amount than the A_o mode across all directions tested, which is in agreement with Guo et al. [18]. In the 0° direction, it can be noticed that the insertion loss is fairly consistent across all propagation distances, with an average A_o drop of 3 dB and an average S_o drop of 18dB. However, despite having a lower amplitude, the S_o mode was found to attenuate less in the HSP than in the GFRP. This is an unexpected discovery, as the increased structural complexity would be thought to cause more scattering and absorption. However, Ono and Gallego [34] reported a similarly complex attenuation behaviour of the S_o mode when investigating propagation in a quasi-isotropic $[0,45,-45,90]_{2s}$ carbon fibre reinforced plastic specimen, where the interaction of the 45° layer resulted in lower attenuation in the off-fibre direction. It is possible that a similar phenomenon is occurring in the HSP due to the interaction between the walls of the aluminium honeycomb and the glass fibre strand direction. If so, it could explain why the maximum attenuation is observed at 30°, since this is both off-fibre direction in the GFLP and off-ribbon direction in the honeycomb, though more research is

needed to understand this particular interaction. Other than one data point at 30°, the A_o mode attenuation is does not change a great deal between the top plate of the HSP and the GFRP. Interestingly, AE recorded on the bottom surface of the HSP did not experience notable attenuation with propagation distance, and in some instances displayed increasing amplitudes with propagation distance. This unusual behaviour could be explained by the fact that, whilst AE in the bottom plate will diminish in amplitude as it propagates over longer distances, longer distances also allow for more energy to be transmitted from the top surface.

4.2. Laser Vibrometry Scanning

4.2.1 GFLP

The laser vibrometer measures the velocity of the surface, thus, the raw data was integrated in order to obtain the surface displacement, as shown in the example waveforms presented in Figure 20. Lamb waves with average dominant frequency components 93.19 kHz for S_o mode and 32.04 kHz for A_o mode. Furthermore, another A_o mode frequencies appeared at 50 kHz due to the excitation utilised. These findings corroborate the findings from the AE testing.

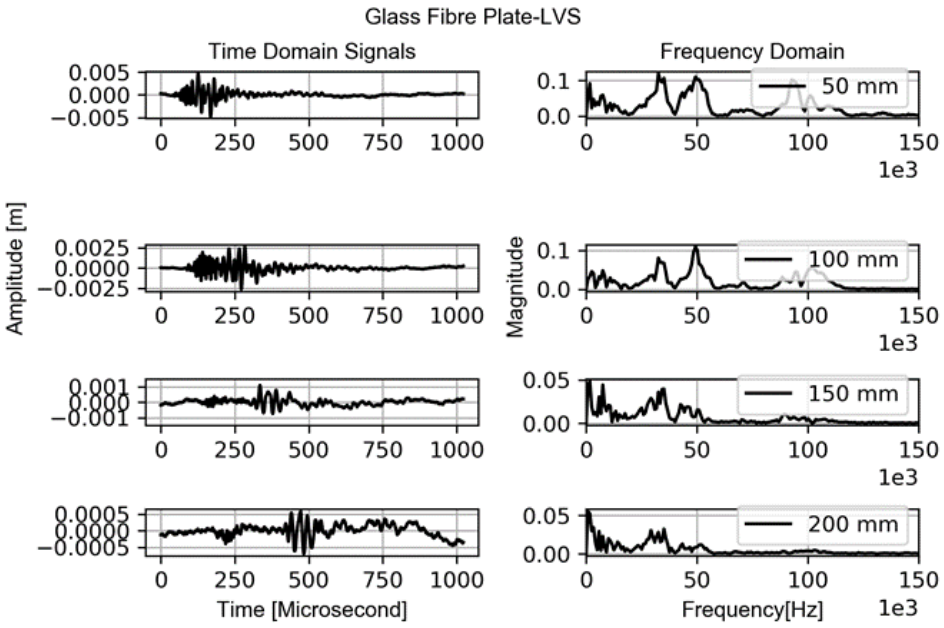

Figure 190. LVS acquired waveforms from GFLP in time and frequency domains in 0° direction at 50, 100, 150, and 200mm

4.2.2. HSP

For the HSP, Figure 21 presents an example of the waveforms in the front plate, when the exciting transducer was also bonded to the front plate. The flexural, A_o Lamb wave component can be seen, with a dominant frequency at 25 kHz, though the amplitude of the

So mode was too diminished to be identified, even when investigating the in-plane motions (e.g. scanning velocity in x and y directions.

Unfortunately, due to the experimental setup, when the transducer was bonded to the back side of the HSP it was not able to inject sufficient energy into the HSP for any recognisable waveform data to be recorded by the vibrometer on the front side. This is in contrast to the results in Section 4.1.3, showing that the energy of the H-N source exceeded that of the piezo actuator used in the vibrometer study. This raises further concerns about the ability of AE to monitor through thickness damage in HSP structures, as the attenuation is so great that smaller signals which could be indicative of damage may not be detected by sensors if they are on the opposing plate, even for very small propagation distances.

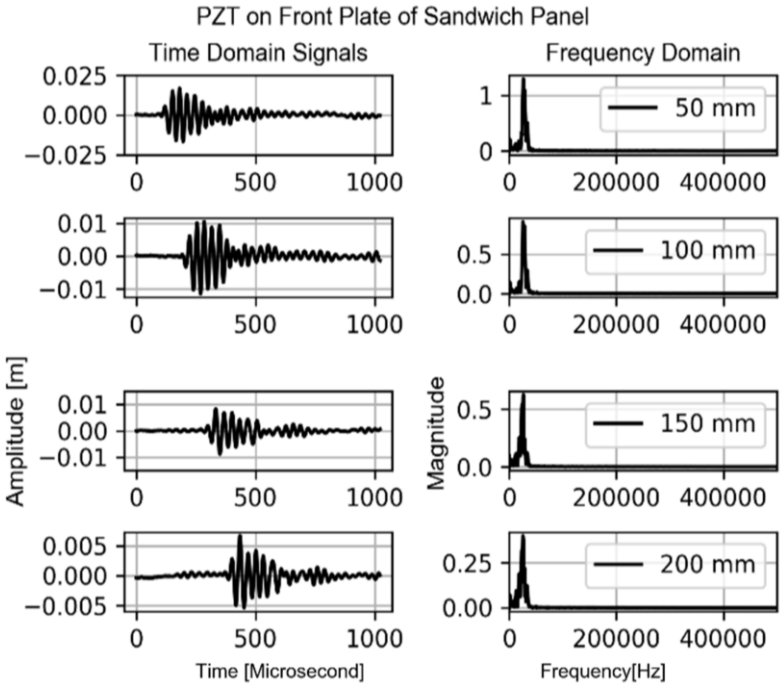

Figure 201. LVS acquired waveforms from HSP front plate (with sensor on front plate) in time and frequency domains in 0^o direction at 50, 100, 150, and 200mm

5. Conclusions

This study offers a comprehensive investigation of AE wave propagation in both a GFLP and HSP using an H-N method and LVS. Through-thickness propagation in HSP structures was investigated in-depth for the first time. The honeycomb cells were found to act as a conduit for AE energy, allowing signals to be recorded by a sensor on the surface opposite to that on which the H-N source was generated. AE propagated as Lamb waves in the GFLP and in the top and bottom surfaces of the HSP, despite the addition of the honeycomb layer, i.e. the HSP cannot be considered as a single propagating medium with one through-thickness propagation mode. However, the Lamb waves in the bottom plate of the HSP (the receiving side) were heavily A_o mode dominant, with severely attenuated S_o mode. This was

thought to be due to the out-of-plane nature of the energy transfer from the honeycomb cells to the bottom surface.

S_o velocity in the GFLP followed the conventional behaviour relying upon the fibre direction while the A_o velocity is independent of fibre direction. Interestingly, despite the addition of the honeycomb layer, which increases the out-of-plane stiffness of the HSP compared to the GFLP on a macro scale, the A_o velocity in the top surface of the HSP was found to be close to that in the GFLP. On the other hand, S_o velocity in the top surface of the HSP displayed starkly different trends than those seen in the GFLP, with maximum velocities of 3927 m/s and 3893 m/s occurring in the 15^o and 75^o directions. It was hypothesised that this departure from the usual, fibre-direction-dependant, velocity profile of the S_o mode was due to the honeycomb layer, and that it is likely no coincidence that the 60^o difference in the directions of the maximum S_o velocities match the 60^o angle between the two ribbon directions in a hexagonal honeycomb lattice, which are the directions in which the honeycomb has its highest stiffness.

Attenuation measurements for AE in the HSP were obtained for both the top and bottom surfaces for the first time. This information is of benefit for researchers considering through thickness attenuation for practical monitoring purposes. The insertion loss concept was introduced to describe the loss of signal amplitude due to the addition of the honeycomb layer. It is proved to be a useful measure to understand the geometrical and material effects on the AE wave propagation.

In conclusion, whilst Lamb waves were found to propagate in both the top and bottom surfaces of the HSP, their behaviours have some distinctive differences to those propagating in a monolithic GFLP due to the complex interactions at play. Future research should be devoted to investigating the implications of this work for the AE source location on both plates of the HSP and to develop a numerical model that is able to investigate the wave energy leakage phenomena through the cells.

Acknowledgments

This work is funded through PhD project entitled “Investigation of Honeycomb Composite Structure for Wind Turbine Blades with Acoustics Emissions Damage Assessment” by Newton-Mosharafa Fund in Egypt, I.D: (NMJ 3/18). Many thanks to Stephen Grigg, Frederic Purcell in Cardiff University and Ahmed Barakat in Technische Universität Darmstadt, Germany for their technical suggestions.

Data Availability Statement

The raw/processed data required to reproduce these findings cannot be shared at this time due to technical or time limitations.

References

[1] Belouettar S, Abbadi A, Azari Z, Belouettar R, Freres P. Experimental investigation

of static and fatigue behaviour of composites honeycomb materials using four point bending tests. Compos Struct 2009;87:265–73.

[2] Gibson LJ, Ashby MF. Cellular solids: structure and properties. Cambridge university press; 1999.

[3] Karthikeyan N, Anand RB, Suthakar T, Barhate S. Materials, Innovations and Future Research Opportunities on Wind Turbine Blades—Insight Review. Environ Prog Sustain Energy 2019;38.

[4] Yang Y, Li B, Chen Z, Sui N, Chen Z, Saeed M-U, et al. Acoustic properties of glass fiber assembly-filled honeycomb sandwich panels. Compos Part B Eng 2016;96:281–6.

[5] Wang Z. Recent advances in novel metallic honeycomb structure. Compos Part B Eng 2019.

[6] Sadighi M, Dehkordi AA, Khodambashi R. A Theoretical and Experimental Study of Failure Maps of Sandwich Beams with Composite Skins and Honeycomb Core. AUT J Model Simul 2010;42:37–47.

[7] Grosse CU, Ohtsu M. Acoustic emission testing. Springer Science & Business Media; 2008.

[8] Non-Destructive TJS for, Inspection. Practical Acoustic Emission Testing. Japan: Springer; 2016.

[9] Ono K. Acoustic emission. Springer Handb. Acoust., Springer; 2014, p. 1209–29.

[10] Xu D, Liu PF, Chen ZP. Damage mode identification and singular signal detection of composite wind turbine blade using acoustic emission. Compos Struct 2020;255:112954.

[11] Nsengiyumva W, Zhong S, Lin J, Zhang Q, Zhong J, Huang Y. Advances, limitations and prospects of nondestructive testing and evaluation of thick composites and sandwich structures: A state-of-the-art review. Compos Struct 2020;256:112951.

[12] Aryan P, Kotousov A, Ng CT, Cazzolato BS. Lamb wave characterisation and damage imaging for isotropic plate-like structures using 3D laser vibrometry 2014.

[13] Friedrich L, Colpo A, Maggi A, Becker T, Lacidogna G, Iturrioz I. Damage process in glass fiber reinforced polymer specimens using acoustic emission technique with low frequency acquisition. Compos Struct 2021;256:113105.

[14] Zhou W, Zhao W, Zhang Y, Ding Z. Cluster analysis of acoustic emission signals and deformation measurement for delaminated glass fiber epoxy composites. Compos Struct 2018;195:349–58.

[15] Hafizi ZM, Epaarachchi J, Lau KT. An investigation of acoustic emission signal attenuation for monitoring of progressive failure in fiberglass reinforced

composite laminates. Int J Automot Mech Eng 2013;8:1442–56.

[16] Wu Y, Perrin M, Pastor M-L, Casari P, Gong X. On the determination of acoustic emission wave propagation velocity in composite sandwich structures. Compos Struct 2020:113231.

[17] Sikdar S, Mirgal P, Banerjee S, Ostachowicz W. Damage-induced acoustic emission source monitoring in a honeycomb sandwich composite structure. Compos Part B Eng 2019;158:179–88.

[18] Guo N, Lim MK. Lamb waves propagation in aluminum honeycomb structures. Rev. Prog. Quant. Nondestruct. Eval., Springer; 1996, p. 323–30.

[19] Baid H, Schaal C, Samajder H, Mal A. Dispersion of Lamb waves in a honeycomb composite sandwich panel. Ultrasonics 2015;56:409–16.

[20] Bai F, Gagar D, Foote P, Zhao Y. Comparison of alternatives to amplitude thresholding for onset detection of acoustic emission signals. Mech Syst Signal Process 2017;84:717–30.

[21] Akaike H. Information theory and an extension of the maximum likelihood principle. Sel. Pap. hirotugu akaike, Springer; 1998, p. 199–213.

[22] Madarshahian R, Ziehl P, Todd MD. Bayesian Estimation of Acoustic Emission Arrival Times for Source Localization. Model Valid. Uncertain. Quantif. Vol. 3, Springer; 2020, p. 127–33.

[23] Liu M, Yang J, Cao Y, Fu W, Cao Y. A new method for arrival time determination of impact signal based on HHT and AIC. Mech Syst Signal Process 2017;86:177–87.

[24] Zhou Z, Cheng R, Rui Y, Zhou J, Wang H. An Improved Automatic Picking Method for Arrival Time of Acoustic Emission Signals. IEEE Access 2019;7:75568–76.

[25] Kappatos V, Dermatas E. Neural localization of acoustic emission sources in ship hulls. J Mar Sci Technol 2009;14:248–55.

[26] Su Z, Ye L. Fundamentals and analysis of lamb waves. Identif. Damage Using Lamb Waves, Springer; 2009, p. 15–58.

[27] McCrory JP, Al-Jumaili SK, Crivelli D, Pearson MR, Eaton MJ, Featherston CA, et al. Damage classification in carbon fibre composites using acoustic emission: A comparison of three techniques. Compos Part B Eng 2015;68:424–30.

[28] Song F, Huang GL, Hudson K. Guided wave propagation in honeycomb sandwich structures using a piezoelectric actuator/sensor system. Smart Mater Struct 2009;18:125007.

[29] Laboratory for Active Materials and Smart Structures (LAMSS). LAMSS Products: LAMSS-COMPOSITES Software n.d. me.sc.edu/research/lamss/html/software.html.

[30] Bakshi UA. Telecommunication engineering. Technical Publications; 2009.

[31] Draudvilienė L, Raišutis R, Žukauskas E, Jankauskas A. Validation of dispersion curve reconstruction techniques for the A0 and S0 modes of Lamb waves. Int J Struct Stab Dyn 2014;14:1450024.

[32] Scholey JJ, Wilcox PD, Lee CK, Friswell MI, Wisnom MR. Acoustic emission in wide composite specimens. Adv. Mater. Res., vol. 13, Trans Tech Publ; 2006, p. 325–32.

[33] Aljets D. Acoustic emission source location in composite aircraft structures using modal analysis. University of South Wales (United Kingdom); 2011.

[34] Ono, Kanji, Gallego A. Attenuation of Lamb Waves in CFRP Plates. J Acoust Emiss 2012;30:109–23.